NEOPLASIA
www.neoplasia.com

Volume 20 Number 3 March 2018 pp. 233–243 233

Paracrine Fibroblast Growth Factor Initiates Oncogenic Synergy with Epithelial FGFR/Src Transformation in Prostate Tumor Progression[1,2]

Qianjin Li*, Lishann Ingram*, Sungjin Kim*, Zanna Beharry†, Jonathan A. Cooper‡ and Houjian Cai*

*Department of Pharmaceutical and Biomedical Sciences, College of Pharmacy, University of Georgia, Athens, Georgia 30602; †Department of Chemistry and Physics, Florida Gulf Coast University, Fort Myers, Florida 33965; ‡Fred Hutchinson Cancer Research Center, Seattle, Washington 98109

Abstract

Cross talk of stromal-epithelial cells plays an essential role in both normal development and tumor initiation and progression. Fibroblast growth factor (FGF)-FGF receptor (FGFR)-Src kinase axis is one of the major signal transduction pathways to mediate this cross talk. Numerous genomic studies have demonstrated that expression levels of FGFR/Src are deregulated in a variety of cancers including prostate cancer; however, the role that paracrine FGF (from stromal cells) plays in dysregulated expression of epithelial FGFRs/Src and tumor progression *in vivo* is not well evaluated. In this study, we demonstrate that ectopic expression of wild-type FGFR1/2 or Src kinase in epithelial cells was not sufficient to initiate prostate tumorigenesis under a normal stromal microenvironment *in vivo*. However, paracrine FGF10 synergized with ectopic expression of epithelial FGFR1 or FGFR2 to induce epithelial-mesenchymal transition. Additionally, paracrine FGF10 sensitized FGFR2-transformed epithelial cells to initiate prostate tumorigenesis. Next, paracrine FGF10 also synergized with overexpression of epithelial Src kinase to high-grade tumors. But loss of the myristoylation site in Src kinase inhibited paracrine FGF10-induced prostate tumorigenesis. Loss of myristoylation alters Src levels in the cell membrane and inhibited FGF-mediated signaling including inhibition of the phosphotyrosine pattern and FAK phosphorylation. Our study demonstrates the potential tumor progression by simultaneous deregulation of proteins in the FGF/FGFRs/Src signal axis and provides a therapeutic strategy of targeting myristoylation of Src kinase to interfere with the tumorigenic process.

Neoplasia (2018) 20, 233–243

Introduction

Cross talk of stromal-epithelial cells plays an essential role in both physiological development and tumor initiation and progression [1,2]. A considerable amount of evidence has demonstrated that fibroblast growth factor (FGF)/FGF receptor (FGFR) signaling is highly deregulated in a variety of cancers including prostate cancer [3–7]. Activation of FGFR in epithelial cells initiates prostate adenocarcinoma [8]. Additionally, this signaling axis mediates cross talk of tumorigenic cells with their microenvironment and facilitates tumor progression including prostate bone metastasis [9].

Src family kinases (SFKs) are a group of nonreceptor tyrosine kinases. The expression and activity of SFK members are commonly upregulated in advanced prostate cancer [10]. SFKs mediate signaling of a variety of cellular receptors including many receptor tyrosine kinases. Our previous study showed that Src kinase played a role in the regulation of the paracrine FGF10-induced prostate tumorigenic process, establishing the important role of an FGF/FGFR/Src axis in cancer progression *in vivo* [11]. Dysregulation of paracrine FGF in

Address all correspondence to: Houjian Cai, Ph.D, Department of Pharmaceutical and Biomedical Sciences, Room 418, Pharmacy South, College of Pharmacy, University of Georgia, Athens, Athens, GA 30602.
E-mail: caihj@uga.edu

[1] Financial support: This work was supported by NIH (R01CA172495) and DOD (W81XWH-15-1-0507) to H. Cai, and NIH (R01GM109463) to J. A. Cooper.
[2] Conflict of interest: The authors disclose no potential conflicts of interest.
Received 7 November 2017; Revised 7 January 2018; Accepted 11 January 2018

© 2018 The Authors. Published by Elsevier Inc. on behalf of Neoplasia Press, Inc. This is an open access article under the CC BY-NC-ND license (http://creativecommons.org/licenses/by-nc-nd/4.0/).
1476-5586
https://doi.org/10.1016/j.neo.2018.01.006

the tumor microenvironment and autonomous FGFRs and Src are common oncogenic events in advanced prostate tumors [10,12,13]; however, the synergistic effect of the FGF/FGFRs/Src axis is understudied in cancer progression.

Several mouse models have been utilized to study the deregulation of FGF/FGFR signaling in prostate cancer. Wang et al. (2003) demonstrated that FGFR1 (K656E), a constitutively active FGFR1 mutant with three times more activity than wild-type FGFR1, induces prostate hyperplasia and prostatic intraepithelial neoplasia after mice reached 6 months age [14]. However, genomic studies indicate that no constitutively active mutations, but amplification of FGFR1 or FGFR2, usually occur in invasive prostate cancer [15,16]. To study the activation of FGFR1, the juxtaposition of CID and kinases 1 (JOCK1) model was created using a recombinant protein. The recombinant protein contains a myristoylation targeting sequence derived from v-Src, the intracellular domain of FGFR1, and two-tandem AP20187 drug binding domains. The recombinant protein was activated by chemically induced dimerization using AP20187 [8,17]. This model nicely simulates the activation of FGFR1, but it does not allow for studying the interaction of the paracrine natural FGF ligand with epithelial FGFRs in tumor progression. The prostate tissue regeneration model utilizes the combination of prostate primary epithelial cells with embryonic urogenital mesenchymal cells to regenerate prostate tissue [18]. This recombination model makes it possible to study the stromal-epithelial cell interactions. Using this model, it has been shown that ectopic expression of paracrine FGF10 in the urogenital mesenchymal cells initiates prostate adenocarcinoma *in vivo* [19,20].

Numerous oncogenic signaling pathways and oncogenic events have been identified in prostate tumors including gene translocation of ERG [21], AR-androgen signaling [22], PTEN/PI3K/AKT, Ras/Raf signaling [23], and many others. The synergy of these oncogenic events, such as Akt and AR [24] and ERG and Akt (or loss of PTEN) [25], significantly promotes cancer progression leading to high-grade tumors. The synergy of Kras and AR [26] and Src and AR [27] could lead to invasive tumors and epithelial-to-mesenchymal (EMT) transition. In this study, we focus on the FGF/FGFR/Src signal axis in prostate cancer and investigate the oncogenic synergy of paracrine FGF10 with cell autonomous FGFR1, FGFR2, and Src in promoting prostate cancer progression. We demonstrate that elevated expression of wild-type FGFR1 and FGFR2 was not sufficient to induce oncogenic transformation; however, it synergizes with paracrine FGF10 to initiate prostate tumors, promote prostate tumor progression, and induce EMT. We also show that paracrine FGF10 synergized with overexpressed epithelial Src kinase resulting in high-grade tumors but not EMT. The FGF10-Src synergy relied on the myristoylation of Src, suggesting that targeting myristoylation of Src kinase might provide a therapeutic approach for inhibiting paracrine FGF10-induced tumorigenesis.

Materials and Methods

Plasmid Construction

Plasmids containing the coding sequence of mouse FGFR1 [Plasmid #14005, FGFR1(IIIc) isoform] and FGFR2 [Plasmid #33248, FGFR2(IIIc) isoform] (with three IgG loops) were obtained from Addgene. The coding sequence of FGFR1 and FGFR2 was subcloned to the bi-cistronic lentiviral vector FUCRW in which RFP is under the control of the CMV promoter and FGFR1/2 is regulated by the human ubiquitin promoter. Similarly, the coding sequence of murine FGF10 was also subcloned into bi-cistronic lentiviral vector FUCGW [11] in which expression of GFP is driven by the CMV promoter, and FGF10 is regulated by the human ubiquitin promoter. FUCRW-Src(WT) and Src(K298M), a kinase-deficient mutant, were created previously [27]. The Src(G2A) mutant, a loss-of-myristoylation mutation, was created by PCR by introducing a point mutation at Gly2 and subsequently cloned in the FUCRW lentiviral vector.

Lentivirus was generated by co-transfecting plasmids expressing the gene of interest and the packaging vectors MDL, VSV, and REV in HEK293T cells. Virus infection was performed as previously described [18]. Lentivirus usage followed the guidelines and regulations of the University of Georgia.

Cell Culture

SYF1 ($Src^{-/-}Yes^{-/-}Fyn^{-/-}$) and HEK293T were purchased from American Type Culture Collection in September 2013. SYF1 cells were transduced with Src(WT), Src(G2A), or Src(K298M) by lentiviral infection to generate stable cell lines. All cell lines were cultured in American Type Culture Collection–recommended medium and temperature.

Prostate Regeneration Assay

C57BL/6J and $CB.17^{SCID/SCID}$ (SCID) mice were purchased from Taconic (Hudson, NY). Primary prostate cells were isolated from 8- to 12-week-old male C57BL/6J mice. Depending on the experimental settings, freshly isolated prostate primary cells were transduced with FGFR1, FGFR2, Src(WT), or Src(G2A) by lentiviral infection. Urogenital sinus mesenchyme (UGSM) cells were isolated from 16.5-day embryos of C57BL/6J mice and transduced with control vector or FGF10 by lentiviral infection. The transduced prostate primary cells (2×10^5 cells/graft) or freshly isolated prostate cells were combined with FGF10 or control UGSM (4×10^5 cells/graft). The cell mixture was resuspended in 20 μl of collagen type I (pH 7.0) (BD Biosciences). After overnight incubation, grafts were implanted under the kidney capsule of SCID male mice. Grafts were harvested after 8-week incubation.

SCID mice carrying the paracrine FGF10-induced prostate tumors 4 weeks after implantation were treated with dasatinib or control vehicle for 4 weeks. Dasatinib was dissolved in 80 mmol/L citrate buffer (pH 3.0) with 5% DMSO. A dose of 15 mg/kg body weight/day was given at 24-hour intervals to the mice using a 20-gauge gavage needle [27]. The control group was given an equal volume of diluent buffer by gavage.

Real-Time PCR

UGSM cells were infected with lentivirus and cultured for 5 days. Total RNA was isolated using the RNeasy Kit (QIAGEN) following the protocol of the manufacturer. A total of 1.5 μg of total RNA was used for reverse transcription to generate complementary DNA in a 20-μl reaction with a high-capacity cDNA reverse transcription kit (Life Technologies). The RT products were diluted 30 times with distilled H_2O, and 2 μl was used as template for each real-time PCR. The reactions were performed using the PerfeCTa SYBR Green FastMix (Quanta Biosciences), and the thermal cycling conditions were an initial denaturation step at 95°C for 1 minute and 40 cycles at 95°C for 10 seconds and 60°C for 50 seconds. The experiments were carried out in triplicate. The relative quantification in fold changes of gene expression was obtained by $2^{-\Delta\Delta Ct}$ method with GAPDH as the

internal reference gene. The primers used for RT-PCR were FGF10-F (CAGTGGAAATCGGAGTTGTT) and FGF10-R (CCTTCT TGTTCATGGCTAAGT), and GAPDH-F (AGGTCGGTGT GAACGGATTTG) and GAPDH-R (TGTAGACCATGTAGTT GAGGTCA).

Immunohistochemistry

Formalin-fixed/paraffin-embedded specimens were sectioned at 5-μm thickness and mounted on positively charged slides. Sections were stained with hematoxylin and eosin (H&E) for histology analysis. Immunohistochemistry was performed using a standard protocol as previously described [28]. For detection of AR and Src expression, primary antibodies for AR (Santa Cruz Biotechnology, SC-816, 1:200) and Src (Cell Signaling, 2109, 1:250) were used and detected with the EnVision+ system (Dako). For immunofluorescent analysis, sections were incubated with primary antibodies against vimentin (Novus Biologicals, NB300-223, 1:250), E-cadherin (Cell Signaling, 3195, 1:250), CK5 (BioLegend, 905501, 1:500), or CK8 (BioLegend, 904801, 1:1000). Expression was detected by Alexa-594– or Alexa-488–conjugated secondary antibodies (Molecular Probes; 1:1000) and DAPI (Vector Laboratories) nucleus staining. The images were taken by a fluorescent microscopy with a CCD camera.

Click Chemistry for Detection of Src Myristoylation

The details of the Click chemistry assay were described previously [29]. In this study, SYF1 ($Src^{-/-}Yes^{-/-}Fyn^{-/-}$) cells expressing Src(WT) or Src(G2A) were cultured in DMEM with 2% fatty acid-free BSA containing 60 μM myristic acid-azide for 24 hours. Cells were washed twice with PBS and lysed on ice for 30 minutes with M-PER lysis buffer (Thermo Fisher) containing protease inhibitors. Protein lysates were collected by centrifugation at 14,000 rpm for 20 minutes, and protein concentration was determined using the Bio-Rad protein assay kit. Click chemistry was carried out with 40 μg of protein lysates, CuSO4 (1 mM), tris(2-carboxyethyl)phosphine (1 mM), tris(benxyltriazolylmethyl)amine (0.1 mM), and the capture reagent (0.1 mM of alkyne-biotin, Invitrogen). After incubation at room temperature for 1 hour in the dark, samples were resolved by SDS-PAGE. Azide-labeled myristoylated proteins were detected by streptavidin-HRP using Western blotting.

Protein Fractionation

Protein fractionation for isolation of cytosol and cell membrane fractions was described previously [30]. Briefly, SYF1 cells expressing Src(WT) or Src(G2A) were cultured in DMEM with 10% FBS and lysed with TNE lysis buffer [50 mM Tris, 150 mM NaCl, 2 mM EDTA (pH 7.4)] and protease inhibitors. The protein lysates were homogenized using a 25-gauge needle syringe (20 strokes) and centrifuged at 14,000 rpm for 20 minutes. The supernatant was collected as the cytosolic fractionation. The pellets were washed twice with TNE lysis buffer and resuspended with TNE lysis buffer containing 60 mM β-octylglucoside. The samples were incubated on ice for 30 minutes and centrifuged at 14,000 rpm for 20 minutes. The supernatant was collected as the cell membrane fractionation. Src, Caveolin-1, and GAPDH were detected by Western blot with specific antibodies.

Western Blot

Cells were lysed in RIPA buffer [137 mM NaCl, 20 mM Tris-HCl (pH 7.4), 10% glycerol, 1% Triton X-100, 0.5% sodium deoxycholate, 0.1% SDS, 2 mM EDTA protease inhibitor cocktail (Millipore, 539137), phosphatase inhibitor cocktail (Sigma-Aldrich, P0044 and P5726)] for 20 minutes on ice. After short sonication, cell lysates were centrifuged, and the supernatants were collected. Proteins were resolved on 10% SDS-polyacrylamide gels and transferred onto nitrocellulose membranes (Bio-Rad). The membrane was blocked with 5% milk powder (Lab Scientific) in 1× TBS containing 1% Tween-20 (TBST) for 1 hour, washed with TBST, and incubated with the specific antibodies overnight. Antibodies to FGFR1 (Cat# 9740), FGFR2 (Cat# 11835), Src (Cat# 2108), p-Src (Y416) (Cat# 2101), FAK (Cat# 3285), p-FAK (Y925) (Cat# 3284), GAPDH (Cat# 5174), and Caveolin-1 (Cat# 3238) were from Cell Signaling Technology. The antibody to ERK2 (Cat# sc-154) was from Santa Cruz Biotechnology. The antibody to phosphotyrosine (pY) was form Millipore (clone 4G10, Cat#05-321), and the γ-tubulin antibody (Cat# T6557) was from Sigma-Aldrich.

Results

Ectopic Expression of FGFR1 in Primary Prostate Epithelial Cells Is Not Sufficient to Induce Prostate Tumorigenesis But Synergizes with Paracrine FGF10 to Induce EMT

Amplification of FGFR1/2, but not constitutively active mutants, has been identified in genomic studies of prostate tumors [12,15]. To recapitulate the role of the amplification of wild-type FGFR1/2 in tumorigenesis, lentiviral vectors expressing FGFR1 (IIIc isoform), FGFR2 (IIIc isoform), or FGF10 were constructed (Figure 1*A*). Expression levels of FGFR1 (Figure 1*B*), FGFR2 (IIIc isoform) (Figure 1*C*), and FGF10 (Figure 1*D*) were confirmed by Western blot or real-time PCR.

To examine aberrant expression of FGFR1 in mediation of prostate tumorigenesis *in vivo*, primary prostate epithelia cells were transduced with control vector or FGFR1 by lentiviral infection. Additionally, UGSM cells were transduced with FGF10 by lentiviral infection. Prostate epithelia with ectopic expression of FGFR1 or control vector were combined with paracrine FGF10 or control vector transduced UGSM cells, and grafts were subjected to the prostate tissue regeneration assay *in vivo* [18] (Figure 1*E*). As expected, paracrine FGF10 induced adenocarcinoma in the PrECs-Control + FGF10-UGSM group. The transformation was multifocal, likely due to the different amount of FGF10 expression locally [11,20]. Paracrine FGF10-induced acini showed an expansion of $CK8^+$ luminal cells with no alteration of $CK5^+$ basal cells located at the basal compartment. Tumorigenic cells expressed androgen receptor and E-cadherin, but not vimentin, suggesting epithelial tumorigenic characteristics. However, overexpression of FGFR1 in epithelial cells showed normal regenerated prostate tubules. RFP in prostate tubules indicated successful transduction. Similar to those in the control group, the regenerated tubules were comprised of a single layer of $CK8^+$ luminal cells and $CK5^+$ basal cells. Epithelial cells in the regenerated tubules expressed E-cadherin (Figure 1*F*). These data suggested that unlike paracrine FGF10 expression, ectopic expression of the wild-type FGFR1 is not sufficient to induce prostate tumorigenesis.

In contrast to regenerated tissues derived from PrECs-control, FGFR1 + GFP-UGSM, or PrECs-control + FGF10-UGSM, tumorigenic cells in the regenerated tissues derived from PrECs-FGFR1 + FGF10-UGSM (RFP^+) were not organized into any ductal structure and showed mild expression of CK8 but not CK5. Some tumorigenic cells co-expressed E-cadherin$^+$ and

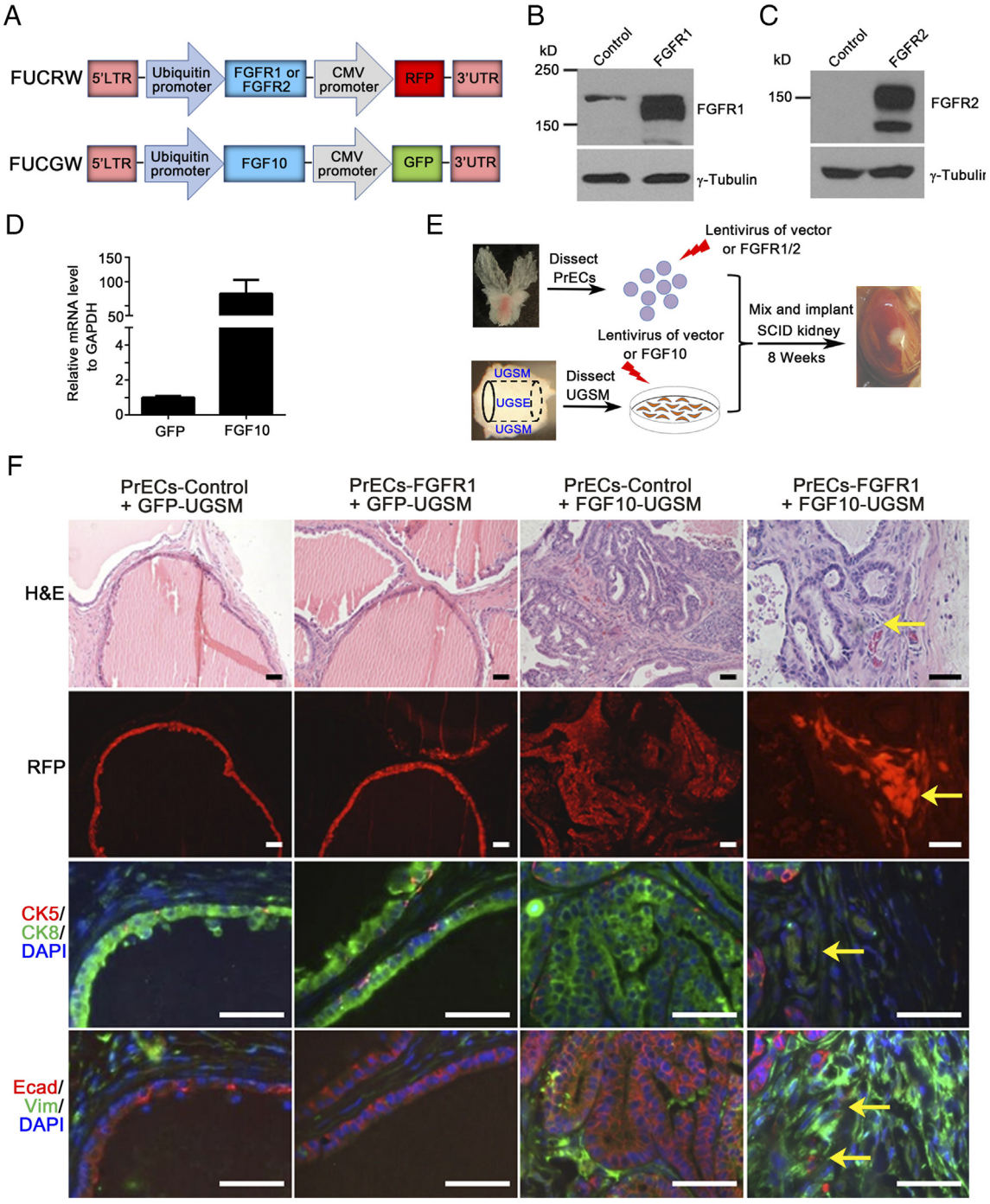

Figure 1. Overexpression of epithelial wild-type FGFR1 synergizes with paracrine FGF10 to induce EMT. (A) Diagram of the bi-cistronic lentiviral vector for the aberrant expression of FGFR1, FGFR2, FGF10, or Src. While the oncogenic gene was controlled by the ubiquitin promoter, RFP or GFP was regulated by the CMV promoter. (B) 293 T cells were transduced with control vector, FGFR1, or FGFR2 by lentiviral infection. The protein lysates were harvested for immunoblotting. The expression levels of FGFR1 or FGFR2, and γ-tubulin were examined by Western blot. Aberrant expression levels of FGFR1 and FGFR2 were confirmed. (C) UGSM cells were transduced with control vector or FGF10 by lentiviral infection. Total mRNA was extracted for the analysis of FGF10 expression by RT-PCR. FGF10 was highly expressed in FGF10-UGSM cells. (D) Diagram for evaluation of FGFR1/2 overexpression in epithelium and aberrant paracrine FGF10-induced tumorigenesis by the prostate tissue regeneration assay *in vivo*. Freshly isolated prostate epithelial cells were transduced with control vector (FUCRW), FGFR1, or FGFR2 by lentiviral infection. UGSM cells were isolated from 16.5-day-old mouse embryos. UGSM cells were transduced with GFP (control) or FGF10 by lentiviral infection. The FGFR1/2-transduced prostate epithelial cells were combined with GFP- or FGF10-UGSM. The combined cells were mixed with collagen and implanted under SCID mouse kidney capsule. The regenerated prostate tissues were harvested after 8-week incubation. (E) The regenerated prostate tissues derived from the experimental groups including PrECs-control + GFP-UGSM, PrECs-FGFR1 + GFP-UGSM, PrECs-control + FGF10-UGSM, and PrECs-FGFR1 + FGF10-UGSM were analyzed for H&E, RFP signal, and IHC staining of CK5 (red)/CK8 (green)/DAPI (blue), and E-Cadherin (red)/vimentin (green)/DAPI (blue). Scale bar, 100 μm. The coexpression of E-Cadherin (red), vimentin (green), and DAPI staining (blue) in tissues from PrECs-FGFR1 + FGF10-UGSM group are presented in Figure S1.

vimentin$^+$ (Figure 1*F* and Figure S1), suggesting that the cells with ectopic expression of FGFR1 under the induction of FGF10-UGSM underwent EMT.

Ectopic Expression of FGFR2 in Primary Prostate Epithelial Cells Is Not Sufficient to Induce Prostate Tumorigenesis But Synergizes with Paracrine FGF10 to Induce EMT

The transformation potential of ectopic expression of FGFR2 (IIIc isoform) and the synergy with paracrine FGF10 were also examined using the prostate tissue regeneration assay. Normal primary prostate cells or FGFR2 transduced cells were combined with FGF10-UGSM cells in the prostate tissue regeneration assay (Figure 1*E*). As expected, while regenerated tissues derived from PrECs-control + GFP-UGSM contained normal tubules, PrECs-control + FGF10-UGSM tissues showed high-grade adenocarcinoma. The FGF10-induced tumors were comprised of disorganized ductal cells expressing CK8 in luminal cells and CK5 at the basal membrane. The normal or transformed epithelial cells were E-cadherin$^+$ and vimentin$^-$ (Figure 2). Similar to FGFR1 transformed tubules or PrECs-control + GFP-UGSM, regenerated tissues derived from PrECs-FGFR2 + GFP-UGSM group were comprised of normal tubules including the expression of CK8 luminal marker, CK5 basal marker, and E-cadherin in epithelial cells (Figure 2), suggesting that ectopic expression of FGFR2 does not sufficiently induce transformation *in vivo*. In contrast, the regenerated tissues from PrECs-FGFR2 + FGF10-UGSM were comprised of sheets of tumorigenic cells (RFP$^+$). These cells did not express CK8 or CK5 but co-expressed E-cadherin and vimentin (Figure 2, and Figure S2). The data indicate that the synergy of paracrine FGF10 with ectopic expression of FGFR2 in epithelia in the FGF/FGFR signaling axis leads to invasive tumors.

Ectopic Expression of FGFR2 Sensitizes Paracrine FGF10-Induced Prostate Tumors

Although overexpression of wild-type FGFRs alone was not sufficient to induce prostate tumorigenesis, we examined if

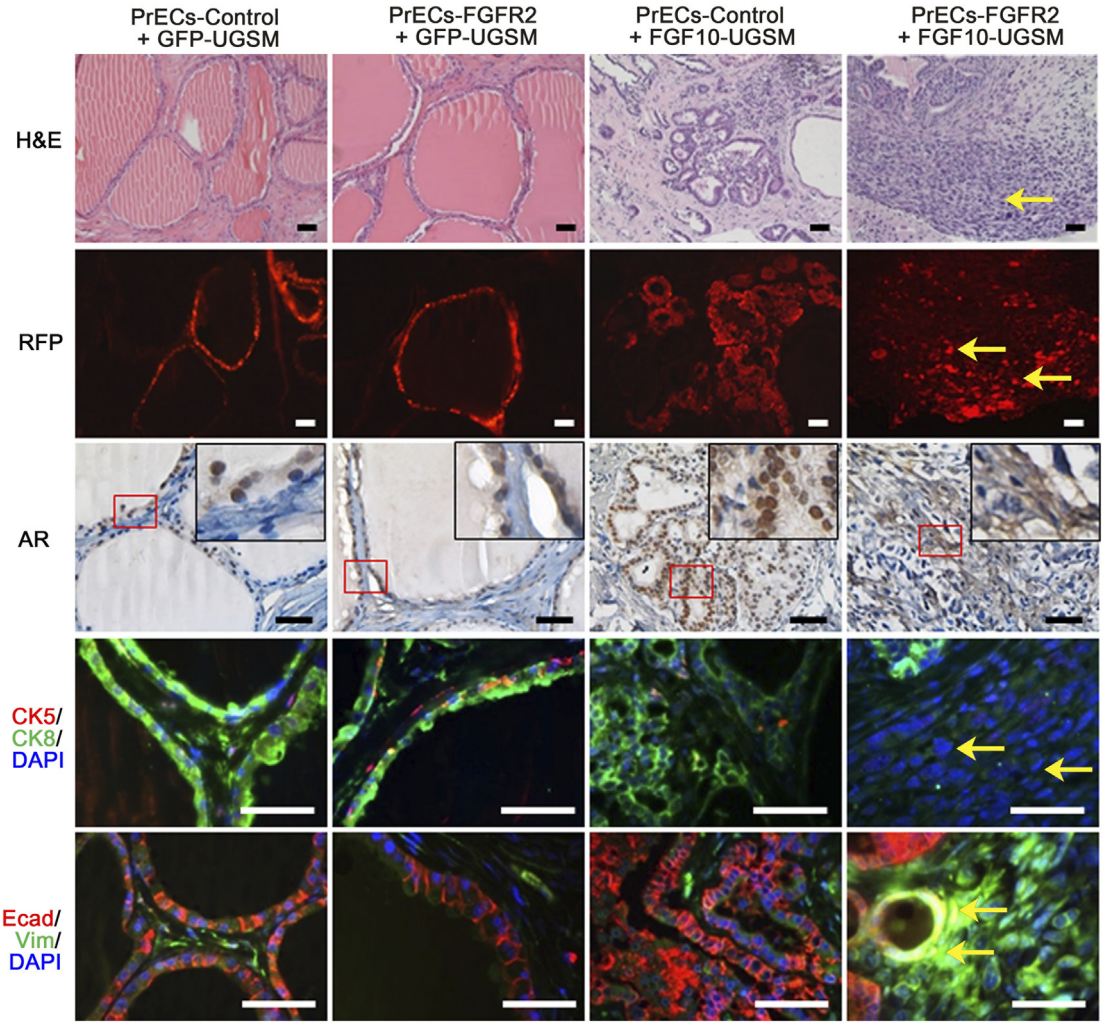

Figure 2. Overexpression of epithelial wild-type FGFR2 synergizes with paracrine FGF10 to induce EMT. Freshly isolated prostate cells were transduced with control vector or FGFR2 by lentiviral infection as shown in the diagram of Figure 1*D*. The transduced epithelial cells were mixed with GFP-UGSM or FGF10-UGSM. The regenerated prostate tissues derived from PrECs-control + GFP-UGSM, PrECs-FGFR2 + GFP-UGSM, PrECs-control + FGF10-UGSM, and PrECs-FGFR2 + FGF10-UGSM were analyzed for H&E staining, RFP signal, and IHC staining of AR, CK5 (red)/CK8 (green)/DAPI (blue), and E-Cadherin (red)/vimentin (green)/DAPI (blue). Yellow arrow indicates FGFR2 transformed tissue. Scale bar, 100 μm. The coexpression of E-Cadherin (red), vimentin (green), and DAPI staining (blue) in tissues from PrECs-FGFR2 + FGF10-UGSM group is presented in Figure S2.

overexpression of FGFR2 in epithelial cells sensitized the cells to a low dose of paracrine FGF10 to cause tumorigenesis. Primary prostate cells and UGSM cells were transduced with FGFR2 and FGF10 by lentiviral infection, respectively. The FGFR2 transduced cells were combined with 100% GFP-UGSM (control) or a mixture of 25% FGF10-UGSM cells and 75% normal UGSM cells (creating a low dosage of paracrine FGF10 from stromal cells) (Figure 3*A*). As expected, the regenerated prostate tissues derived from PrECs-control or FGFR2 with 100% GFP-UGSM were comprised of normal tubules with expression of a single layer of CK8$^+$ luminal cells and CK5$^+$ cells in the basal membrane (Figure 3*B*). While the regenerated tissues from PrECs-control + 25% FGF10-UGSM showed normal tubules with an increase in branching, the tissues in PrECs-FGFR2 + 25% FGF10-UGSM exhibited low-grade prostatic intraepithelial neoplasia (Figure 3*B*). The transformed tubules contained stratified CK8$^+$ luminal cells and retained the basal cell layer, and some small acini were visible. Additionally, epithelial cells in normal tubules or in the lesion expressed E-cadherin but not vimentin, indicating the

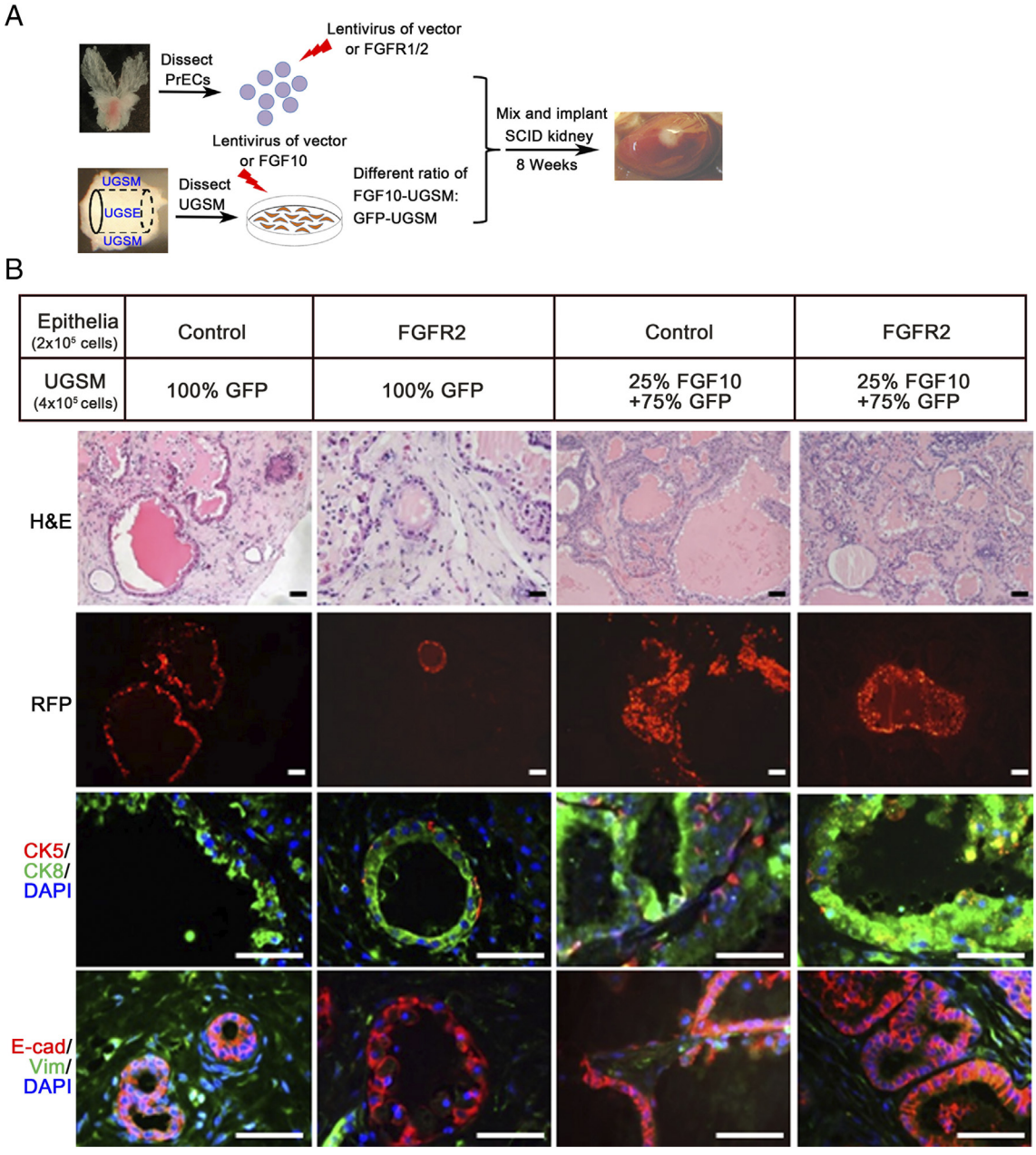

Figure 3. Overexpression of wild-type FGFR2 sensitizes epithelial cells to low-dose paracrine FGF10 for initiation of prostate tumorigenesis. (A) Experimental setup for studying the synergy of a low dosage of paracrine FGF10-induced tumorigenesis with the transformation of FGFR2 (FGFR2c isoform) in epithelia. Freshly isolated prostate cells were transduced with control vector or FGFR2 by lentiviral infection. UGSM cells were transduced with FGF10 or control vector by lentiviral infection. The transduced epithelial cells were mixed with 100% GFP-UGSM (normal UGSM as a control) or 75% control-UGSM + 25% FGF10-UGSM. (B) The regenerated prostate tissues derived from the experimental groups [PrECs-control + GFP-UGSM, PrECs-FGFR2 + GFP-UGSM, PrECs-control + (25% FGF10-UGSM + 75% GFP-UGSM), and PrECs-FGFR2 + (25% FGF10-UGSM + 75% GFP-UGSM)] were analyzed for H&E staining, RFP signal, and IHC staining of CK5 (red)/CK8 (green)/DAPI (blue) and E-Cadherin (red)/vimentin (green)/DAPI (blue). Scale bar, 100 μm.

epithelial feature. These results indicate that FGFR2-transduced cells become sensitized to the low dosage of paracrine FGF10 to induce prostate tumorigenesis.

Inhibition of Src Kinase Activity Suppresses FGF10-Induced Tumorigenesis

Previous studies have shown that Src family kinase members exhibit differential capacities in mediating paracrine FGF10-induced prostate tumorigenesis. For example, epithelial Src kinase is essential for paracrine FGF10-induced tumors [11], suggesting that the FGF/FGFR/Src signaling axis plays an important role in prostate tumor progression. We further examined the activity of Src in FGF10 mediated tumorigenesis using dasatinib, a pharmacological inhibitor of Src kinase activity [31]. Host mice carrying the regenerated prostate tissues of PrECs + GFP or FGF10-UGSM were treated with vehicle control or dasatinib. While dasatinib treatment had no effect on the prostate regeneration process, it inhibited FGF10-induced tumorigenesis (Figure 4). Multiple layers of luminal epithelial cells ($CK8^+$) were less prominent in the FGF10-UGSM group treated with dasatinib (Figure 4), suggesting that Src kinase expression facilitates FGF10-induced tumor progression.

Ectopic Expression of Src Kinase Synergizes with Paracrine FGF10 in Prostate Tumorigenesis

Expression and/or activity of Src kinase are usually highly elevated in advanced prostate cancer [10]. We further examined the potential synergistic effect of epithelial Src with paracrine FGF10 in tumor progression. Of note, varying the ratio of epithelial to FGF10-UGSM cells showed differential pathological phenotypes in the regenerated prostate tissues (Figure S3). While the regenerated tissues containing a 1:2 ratio of epithelium:FGF10-UGSM led to prostate adenocarcinoma, a 1:1 ratio led to branched tubules (Figure S3).

Primary prostate cells were transduced with control or wild-type Src kinase, and the transduced cells were combined with GFP- or FGF10-UGSM in the prostate regeneration assay (Figure S4*A*). As previously reported, regenerated tissues derived from the control or Src(WT) + GFP-UGSM showed normal tubules [27]. Regenerated tissues derived from paracrine FGF10-induced grafts (1:1 ratio of epithelia: FGF10-UGSM) enhanced branching morphogenesis. In contrast, overexpression of Src(WT) in epithelium synergized with FGF10-UGSM, resulting in high-grade adenocarcinoma (Figure S4*B*). Histological analysis showed that the tissues derived from the PrECs-Src + FGF10-UGSM group formed a cluster of acini with an expansion of $CK8^+$ luminal cells and complete or partial $CK5^+$ cells located at the basal membrane and were E-cadherin$^+$, an epithelial characteristic (Figure S4). In contrast, the other tissue groups showed a single layer of $CK8^+$ luminal cells with $CK5^+$ at the basal membrane. The data indicate that ectopic expression of epithelial Src kinase synergizes with paracrine FGF10 in promoting high-grade prostate tumors without induction of EMT, which is a different pathological phenotype to the synergy of paracrine FGF10 with epithelial FGFR1/2(WT).

Loss of Src Myristoylation Inhibits Paracrine FGF10-Induced Tumorigenesis In Vivo

Myristoylation is an important lipid modification for Src kinase activity [32–34]. We further examined the role of Src myristoylation in FGF10-induced tumorigenesis *in vivo*. Overexpression of wild-type Src or the myristoylation defective mutant Src(G2A) was confirmed (Figure 5*A*). Prostate epithelial cells transduced with Src(WT) or Src(G2A) were mixed with FGF10-UGSM or GFP-UGSM cells, and the cell mixtures were used in the prostate regeneration assay. While the weight of regenerated tissues derived from Src(WT) or Src(G2A) + GFP-UGSM had no significant

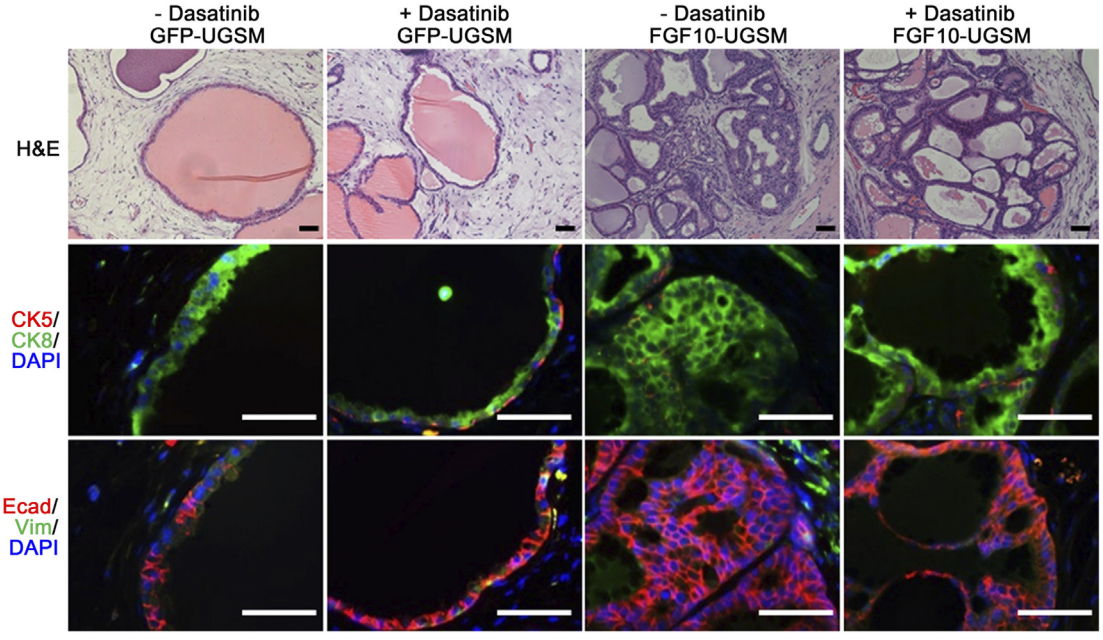

Figure 4. Dasatinib inhibits paracrine FGF10-induced prostate tumorigenesis. Epithelial cells were mixed with GFP- or FGF10-UGSM. The cell mixture was implanted under the kidney capsule of SCID mice. After 4 weeks of incubation, host mice carrying the regenerated grafts were treated with dasatinib by gavage (75 mg/kg). The regenerated prostate tissues were harvested for pathological analysis after 4 weeks of treatment and analyzed for H&E staining, IHC staining of CK5 (red)/CK8 (green)/DAPI (blue) and E-Cadherin (red)/vimentin (green)/DAPI (blue). The 1:1 ratio of epithelial cells to FGF10-UGSM resulted in branched tubules, and the 1:2 ratio led to adenocarcinoma. Pathological analysis indicated that dasatinib inhibits paracrine FGF10 induced tumorigenesis. Scale bar, 100 μm.

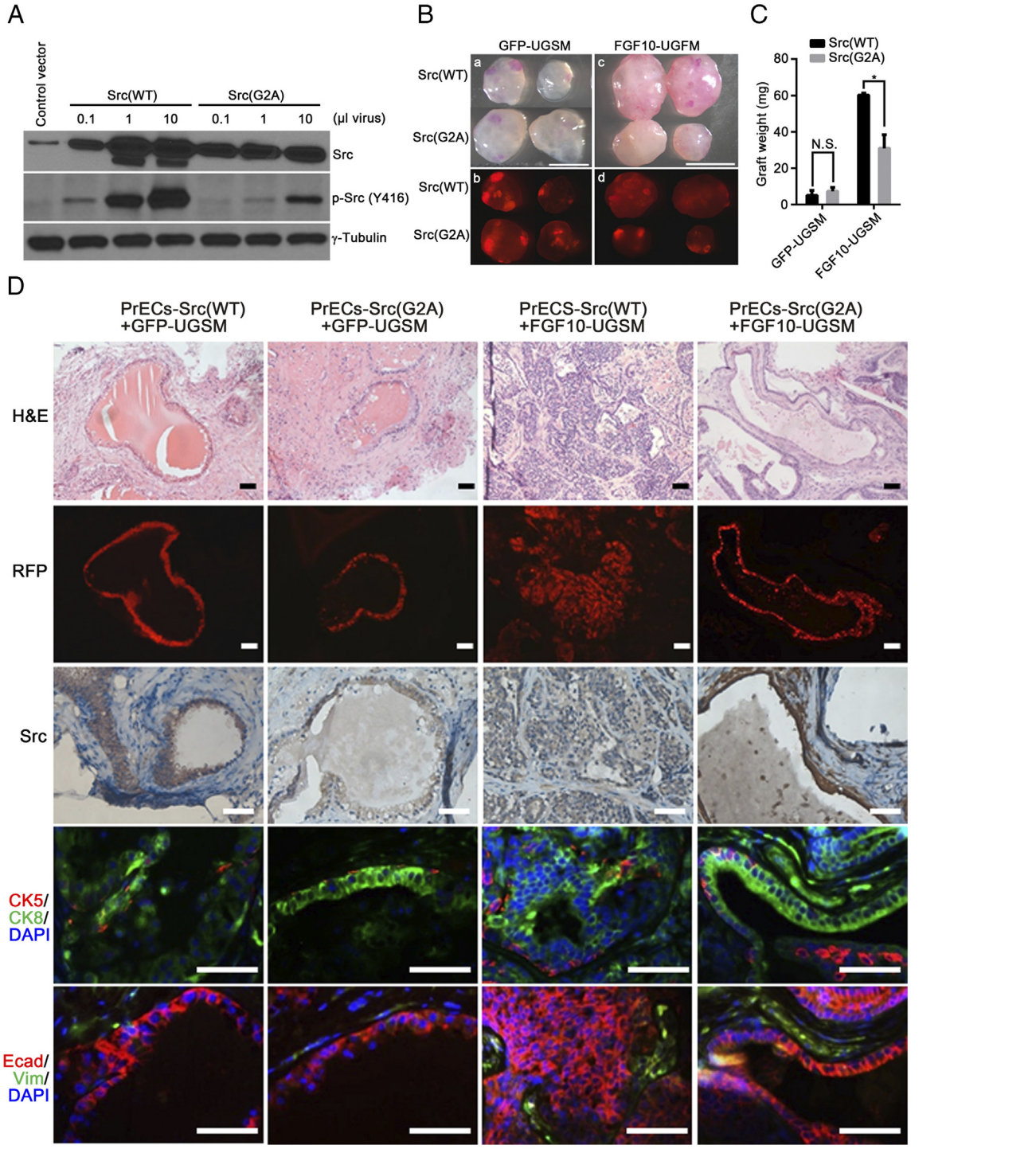

Figure 5. Loss of Src myristoylation inhibits paracrine FGF10-induced tumorigenesis. (A) 293 T cells were transduced with control vector, 0.1, 1, and 10 μL of Src(WT) or Src(G2A) lentivirus. The transduced cells were harvested, and protein lysates were analyzed for the expression levels of Src, phospho-Src and γ-tubulin. (B-C) Phase and RFP fluorescence images (B) and weight (C) of the regenerated prostate tissues derived from PrECs-Src(WT) + GFP-UGSM, PrECs-Src(G2A) + GFP-UGSM, PrECs-Src(WT) + FGF10-UGSM, and PrECs-Src(G2A) + FGF10-UGSM groups. Scale bar, 0.5 mm. Values are mean ± SD. *: $p<0.05$. (D) The regenerated tissues derived from PrECs-Src(WT) + GFP-UGSM, PrECs-Src(G2A) + GFP-UGSM, PrECs-Src(WT) + FGF10-UGSM, and PrECs-Src(G2A) + FGF10-UGSM groups were analyzed for H&E staining, RFP signal, and IHC staining of Src, CK5 (red)/CK8 (green)/DAPI (blue), and E-Cadherin (red)/ vimentin (green)/DAPI (blue). Scale bar, 100 μm.

difference (Figure 5, *B-C*), those derived from PrECs-Src(G2A) + FGF10-UGSM were significantly inhibited in comparison with PrECs-Src(WT) + FGF10-UGSM (Figure 5, *B-C*). RFP fluorescence images indicate the location of transduced Src(WT) or Src(G2A) in the regenerated tissues (Figure 5*B*). Histological analysis showed that the elevated expression of Src kinase was in the RFP^+ tubules. As expected, regenerated tissues from PrECs-Src(WT) or Src(G2A) + GFP-UGSM were comprised of normal tubules with a

single layer of CK8$^+$ luminal cells and CK5$^+$ basal cell layer [27,34]. The epithelial cells were E-cadherin$^+$ and vimentin$^-$. Tissues derived from PrECs-Src(WT)+FGF10-UGSM group showed high-grade adenocarcinoma (Figure 5*D*). Transformed regenerated tissues from this group contained an expansion of CK8$^+$ luminal cells without substantial changes in CK5$^+$ basal cells. However, regenerated tissues derived from epithelia-Src(G2A)+FGF10-UGSM were comprised of normal tubules. The tubules contained a single layer of CK8$^+$ luminal cells with CK5$^+$ basal cells as in the PrECs + GFP-UGSM control group (Figure 5*D*). The data indicate that loss of Src myristoylation inhibits FGF10-induced prostate tumorigenesis, suggesting a potential therapeutic approach of targeting myristoylation of Src kinase to inhibit FGF/FGFRs-mediated tumorigenic potential.

Loss of Src Myristoylation Inhibits Exogenous FGF2-Induced Signaling In Vitro

We further studied the underlying mechanisms which loss of Src myristoylation inhibits FGF/FGFRs mediated tumorigenesis. The Src(G2A) mutant, in which mutation of glycine to alanine at site 2 led to loss of myristoylation of Src kinase, was confirmed by Click chemistry (Figure 6*A*). While levels of Src(WT) kinase were mainly localized in the cell membrane fraction, the majority of Src(G2A) kinase was expressed in the cytosol fraction (Figure 6*B*). Ectopic expression of Src(WT) in SYF1 cells (no endogenous Src expression) significantly elevated tyrosine phosphorylation of proteins between 50 and 75 kDa and between 100 and 150 kDa [detected by anti–phospho-tyrosine antibody (pY)] in comparison with SYF1 cells induced with FGF2. In contrast, similar to Src(K298M), a kinase dead mutant, overexpression of Src(G2A) had minimal induction in phospho-tyrosine bands around 75 kDa or 25 kDa (Figure 6*C*). The data indicate that, similar to Src(K298M), Src(G2A) significantly inhibited FGF2-induced signaling.

The Src(G2A) mutant was also examined in NIH-3T3 cells (with endogenous Src expression). Overexpression of Src(G2A) reduced FGF2-induced signaling including lower levels of phospho-tyrosine proteins and phosphorylation of FAK (Figure 6*D*), suggesting that

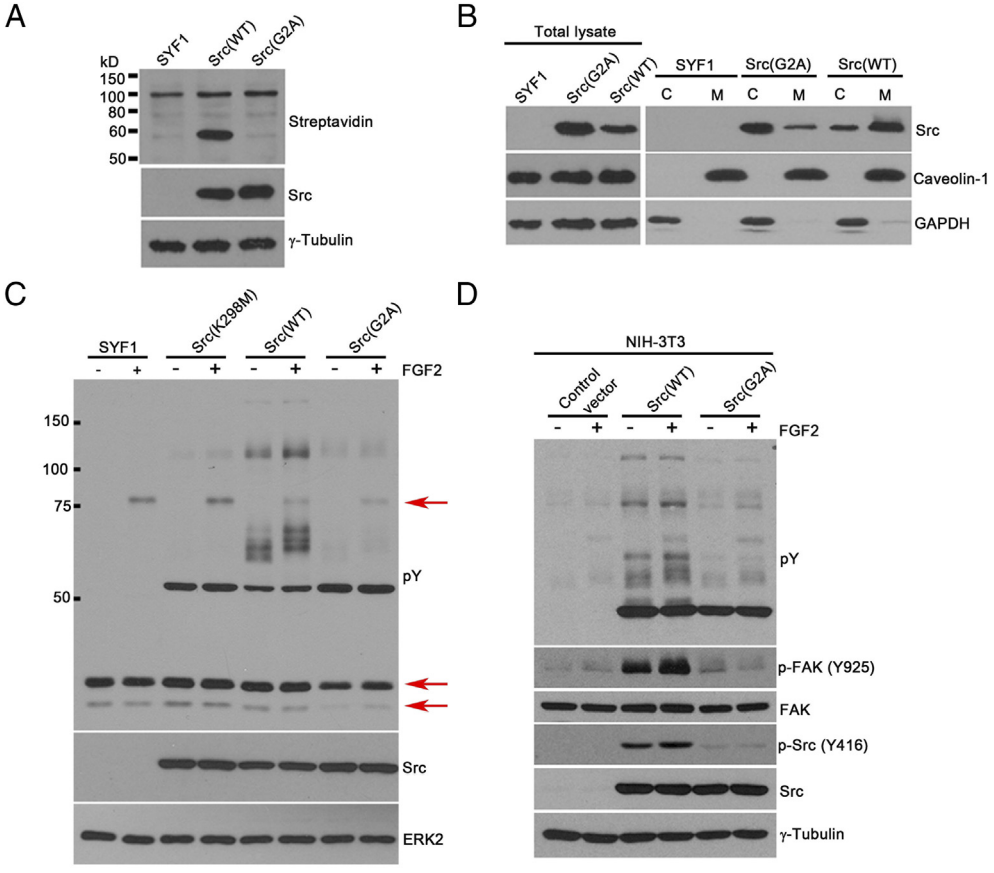

Figure 6. Loss of myristoylation in Src kinase inhibits FGF2 induced signaling *in vitro*. (A) SYF1 (Src$^{-/-}$Yes$^{-/-}$Fyn$^{-/-}$) cells expressing Src(WT) or Src(G2A) were grown in medium containing 50 μM myristic acid-azide for 24 hours. Myristoylated proteins were detected by Click chemistry. Expression levels of Src and tubulin in cell lysates were measured by immunoblotting. (B) SYF1 cells transduced with Src(WT) or Src(G2A) were fractionated into cytosol (C) and cell membrane (M) fractions. Levels of Src kinase were examined in both fractions by immunoblotting. Caveolin-1 and GAPDH were used as markers for total cell membrane fraction (M) and cytosolic fraction (C), respectively. Both markers were used as the loading control for the total lysate analysis. (C) SYF1(Src$^{-/-}$Yes$^{-/-}$Fyn$^{-/-}$) parental cells and SYF1 cells transduced with Src(WT), Src(G2A), or Src(K298M) were grown with/without FGF2 (50 ng/ml) for 10 minutes. Protein lysates were analyzed for phosphorylated tyrosine, Src, and ERK2 levels by immunoblotting. Levels of phosphorylated tyrosine were detected by the anti-phosphotyrosine antibody (4G10). The phosphorylation of bands around 25 kDa and 75 kDa (as indicated by the red arrows) were inhibited in the Src(G2A) groups in comparison with Src(WT) and Src(K298M) group. (D) NIH-3T3 cells transduced with Src(WT), Src(G2A), or control vector were grown with/without FGF2 (50 ng/ml) for 10 minutes. Protein lysates were analyzed for phosphorylated tyrosine (detected by 4G10 antibody), Src, p-Src (Y416), FAK, p-FAK (Y925), and γ-tubulin levels by immunoblotting.

loss of Src myristoylation has a dominant negative effect in blockade of paracrine FGF induced signaling.

Discussion

Our study has demonstrated that the FGF/FGFR/Src signaling axis is important in mediating tumor initiation and progression in prostate cancer. Previous prostate cancer models in the study of FGFRs focused on the simulation of activation of FGFRs. Although amplification of FGFR1 or FGFR2 has been well documented, mutations leading to the activation of FGFRs do not often occur in prostate cancer [12,15]. For example, the translocation of FGFR2 leading to gene fusion of SLC45A3-FGFR2 results in overexpression of FGFR2 [12]. However, our results indicate that ectopic expression of the wild-type FGFR1/2 is not sufficient to induce prostate tumorigenesis under the normal stromal microenvironment. The FGFR2 transformed epithelial cells become sensitized to the amount of paracrine FGF in the microenvironment, leading to transformation. The data emphasize that the dysregulation of the stromal microenvironment is a decisive factor to induce the FGF/FGFR-mediated prostate tumorigenesis. Dysregulated FGF expression plays an essential role in androgen receptor–independent prostate cancer [35].

The activation of FGFR1/2 is an important factor to regulate the EMT in cancer progression. We show that the synergy of paracrine FGF with epithelial wild-type FGFR1/2 in this signaling axis promotes tumor progression and induces EMT *in vivo*. This is in agreement with the induction of activated FGFR1 in another mouse prostate cancer model [8]. FGFR2-induced EMT occurs when tumorigenic cells undergo the isoform switch from FGFR2b to FGFR2c during prostate cancer progression [36]. The isoform switch–induced EMT has also been reported in human dermal fibroblasts [37] and rat bladder carcinoma cells [38]. Mechanistically, FGFR2c-induced transformation inhibits the expression of E-cadherin but increases expression levels of vimentin [37]. FGFR2 expression is associated with twist1-induced cancer progression, invasion, and EMT in gastric adenocarcinoma [39]. FGFR2 also mediates N-cadherin–induced EMT to regulate expression levels of snail, twist1, and slug [40].

Paracrine FGF10 also synergizes with epithelial wild-type Src kinase in the FGF/FGFR/Src signaling axis. Ectopic expression of Src kinase in the epithelium synergizes with paracrine FGF10 and leads to high-grade adenocarcinoma. Src kinase is essential in paracrine FGF10-induced prostate tumorigenesis *in vivo* [11]. Pathologically, FGF10-Src(WT) synergy exhibits a much weaker phenotype than FGF10-FGFR2(WT), suggesting that the participation of other pathways downstream of FGFR also plays important roles for the initiation of EMT. The FGF/FGFR/Src signaling axis is also consistent with numerous *in vitro* studies showing that Src kinase is associated with FGFRs [41]. However, most of the FGF/FGFR models emphasize FGF/FGFR/FRS2-induced MAPK and PI3K pathways [42]. While some models indicate that Src kinase is associated with PLC-gamma signaling [43], others suggest that Src directly interacts with FGFRs [44]. Further delineation of Src kinase in FGF/FGFR downstream signaling will be helpful for understanding FGF/FGFR signaling in cancer progression.

Our study has shown that ectopic expression of the mutant Src(G2A) abolishes FGF10-induced tumorigenesis *in vivo*. Myristoylation has been reported as an important modification for Src kinase to associate with the cytoplasmic membrane [33,45]. Loss of Src myristoylation inhibits its kinase activity and increases protein stability [33]. Dasatinib has been used in clinic trials to target the ATP binding site of Src kinase; however, the beneficial effect is very limited [46]. Our data show that loss of Src myristoylation has a significant inhibitory effect on FGF10-induced oncogenic signaling in comparison with the kinase dead mutant. Therefore, targeting N-myristoylation might represent an important chemotherapeutic approach for inhibiting FGF/FGFR/Src-mediated cancer progression [47]. N-myristoyltransferase catalyzes the myristoylation process [48]. Several compounds have been identified that inhibit the catalytic function of NMT including a myristoyl-CoA analog we have recently discovered [34,49,50]. Further study of these compounds might provide a therapeutic strategy for inhibiting Src kinase activity, thereby blocking FGF/FGFR/Src mediated cancer.

Supplementary data to this article can be found online at https://doi.org/10.1016/j.neo.2018.01.006.

Acknowledgements

We thank Farah Shahin in Dr. Jonathan A. Cooper's lab for providing prostate tissues. This work was supported by grants from NIH (R01CA172495) and DOD (W81XWH-15-1-0507) to H. Cai, and NIH (R01GM109463) to JA. Cooper.

References

[1] Cunha GR, Donjacour AA, Cooke PS, Mee S, Bigsby RM, Higgins SJ, and Sugimura Y (1987). The endocrinology and developmental biology of the prostate. *Endocr Revs* **8**, 338–362.
[2] Hayward SW, Wang Y, Cao M, Hom YK, Zhang B, Grossfeld GD, Sudilovsky D, and Cunha GR (2001). Malignant transformation in a nontumorigenic human prostatic epithelial cell line. *Cancer Res* **61**, 8135–8142.
[3] Katoh M and Nakagama H (2014). FGF receptors: cancer biology and therapeutics. *Med Res Rev* **34**, 280–300.
[4] Feng S, Wang J, Zhang Y, Creighton CJ, and Ittmann M (2015). FGF23 promotes prostate cancer progression. *Oncotarget* **6**, 17291–17301.
[5] Corn PG, Wang F, McKeehan WL, and Navone N (2013). Targeting fibroblast growth factor pathways in prostate cancer. *Clin Cancer Res* **19**, 5856–5866.
[6] Nagamatsu H, Teishima J, Goto K, Shikuma H, Kitano H, Shoji K, Inoue S, and Matsubara A (2015). FGF19 promotes progression of prostate cancer. *Prostate* **75**, 1092–1101.
[7] Dieci MV, Arnedos M, Andre F, and Soria JC (2013). Fibroblast growth factor receptor inhibitors as a cancer treatment: from a biologic rationale to medical perspectives. *Cancer Discov* **3**, 264–279.
[8] Acevedo VD, Gangula RD, Freeman KW, Li R, Zhang Y, Wang F, Ayala GE, Peterson LE, Ittmann M, and Spencer DM (2007). Inducible FGFR-1 activation leads to irreversible prostate adenocarcinoma and an epithelial-to-mesenchymal transition. *Cancer Cell* **12**, 559–571.
[9] Wan X, Corn PG, Yang J, Palanisamy N, Starbuck MW, Efstathiou E, Tapia EM, Zurita AJ, Aparicio A, and Ravoori MK, et al (2014). Prostate cancer cell-stromal cell crosstalk via FGFR1 mediates antitumor activity of dovitinib in bone metastases. *Sci Transl Med* **6**, 252ra122.
[10] Guo Z, Dai B, Jiang T, Xu K, Xie Y, Kim O, Nesheiwat I, Kong X, Melamed J, and Handratta VD, et al (2006). Regulation of androgen receptor activity by tyrosine phosphorylation. *Cancer Cell* **10**, 309–319.
[11] Cai H, Smith DA, Memarzadeh S, Lowell CA, Cooper JA, and Witte ON (2011). Differential transformation capacity of Src family kinases during the initiation of prostate cancer. *Proc Natl Acad Sci U S A* **108**, 6579–6584.
[12] Wu YM, Su F, Kalyana-Sundaram S, Khazanov N, Ateeq B, Cao X, Lonigro RJ, Vats P, Wang R, and Lin SF, et al (2013). Identification of targetable FGFR gene fusions in diverse cancers. *Cancer Discov* **3**, 636–647.
[13] Kwabi-Addo B, Ozen M, and Ittmann M (2004). The role of fibroblast growth factors and their receptors in prostate cancer. *Endocr Relat Cancer* **11**, 709–724.
[14] Wang F, McKeehan K, Yu C, Ittmann M, and McKeehan WL (2004). Chronic activity of ectopic type 1 fibroblast growth factor receptor tyrosine kinase in prostate epithelium results in hyperplasia accompanied by intraepithelial neoplasia. *Prostate* **58**, 1–12.
[15] Bova GS, Kallio HM, Annala M, Kivinummi K, Hognas G, Hayrynen S, Rantapero T, Kivinen V, Isaacs WB, and Tolonen T, et al (2016). Integrated

clinical, whole-genome, and transcriptome analysis of multisampled lethal metastatic prostate cancer. *Cold Spring Harb Mol Case Stud* **2**, a000752.
[16] Mehta P, Robson CN, Neal DE, and Leung HY (2000). Fibroblast growth factor receptor-2 mutation analysis in human prostate cancer. *BJU Int* **86**, 681–685.
[17] Freeman KW, Welm BE, Gangula RD, Rosen JM, Ittmann M, Greenberg NM, and Spencer DM (2003). Inducible prostate intraepithelial neoplasia with reversible hyperplasia in conditional FGFR1-expressing mice. *Cancer Res* **63**, 8256–8263.
[18] Xin L, Ide H, Kim Y, Dubey P, and Witte ON (2003). In vivo regeneration of murine prostate from dissociated cell populations of postnatal epithelia and urogenital sinus mesenchyme. *Proc Natl Acad Sci U S A* **100**(Suppl. 1), 11896–11903.
[19] Memarzadeh S, Cai H, Janzen DM, Xin L, Lukacs R, Riedinger M, Zong Y, DeGendt K, Verhoeven G, and Huang J, et al (2011). Role of autonomous androgen receptor signaling in prostate cancer initiation is dichotomous and depends on the oncogenic signal. *Proc Natl Acad Sci U S A* **108**, 7962–7967.
[20] Memarzadeh S, Xin L, Mulholland DJ, Mansukhani A, Wu H, Teitell MA, and Witte ON (2007). Enhanced paracrine FGF10 expression promotes formation of multifocal prostate adenocarcinoma and an increase in epithelial androgen receptor. *Cancer Cell* **12**, 572–585.
[21] Tomlins SA, Laxman B, Varambally S, Cao X, Yu J, Helgeson BE, Cao Q, Prensner JR, Rubin MA, and Shah RB, et al (2008). Role of the TMPRSS2-ERG gene fusion in prostate cancer. *Neoplasia* **10**, 177–188.
[22] Sadar MD (2011). Small molecule inhibitors targeting the "Achilles' heel" of androgen receptor activity. *Cancer Res* **71**, 1208–1213.
[23] Taylor BS, Schultz N, Hieronymus H, Gopalan A, Xiao Y, Carver BS, Arora VK, Kaushik P, Cerami E, and Reva B, et al (2010). Integrative genomic profiling of human prostate cancer. *Cancer Cell* **18**, 11–22.
[24] Xin L, Teitell MA, Lawson DA, Kwon A, Mellinghoff IK, and Witte ON (2006). Progression of prostate cancer by synergy of AKT with genotropic and nongenotropic actions of the androgen receptor. *Proc Natl Acad Sci U S A* **103**, 7789–7794.
[25] Zong Y, Xin L, Goldstein AS, Lawson DA, Teitell MA, and Witte ON (2009). ETS family transcription factors collaborate with alternative signaling pathways to induce carcinoma from adult murine prostate cells. *Proc Natl Acad Sci U S A* **106**, 12465–12470.
[26] Cai H, Memarzadeh S, Stoyanova T, Beharry Z, Kraft AS, and Witte ON (2012). Collaboration of Kras and androgen receptor signaling stimulates EZH2 expression and tumor-propagating cells in prostate cancer. *Cancer Res* **72**, 4672–4681.
[27] Cai H, Babic I, Wei X, Huang J, and Witte ON (2011). Invasive prostate carcinoma driven by c-Src and androgen receptor synergy. *Cancer Res* **71**, 862–872.
[28] Wu M, Ingram L, Tolosa EJ, Vera RE, Li Q, Kim S, Ma Y, Spyropoulos DD, Beharry Z, and Huang J, et al (2016). Gli transcription factors mediate the oncogenic transformation of prostate basal cells induced by a Kras-androgen receptor axis. *J Biol Chem* **291**, 25749–25760.
[29] Kim S, Yang X, Li Q, Wu M, Costyn L, Beharry Z, Bartlett MG, and Cai H (2017). Myristoylation of Src kinase mediates Src-induced and high-fat diet–accelerated prostate tumor progression in mice. *J Biol Chem* **292**, 18422–18433.
[30] Adam RM, Yang W, Di Vizio D, Mukhopadhyay NK, and Steen H (2008). Rapid preparation of nuclei-depleted detergent-resistant membrane fractions suitable for proteomics analysis. *BMC Cell Biol* **9**, 30.
[31] Nam S, Kim D, Cheng JQ, Zhang S, Lee JH, Buettner R, Mirosevich J, Lee FY, and Jove R (2005). Action of the Src family kinase inhibitor, dasatinib (BMS-354825), on human prostate cancer cells. *Cancer Res* **65**, 9185–9189.
[32] Lacal PM, Pennington CY, and Lacal JC (1988). Transforming activity of ras proteins translocated to the plasma membrane by a myristoylation sequence from the src gene product. *Oncogene* **2**, 533–537.
[33] Patwardhan P and Resh MD (2010). Myristoylation and membrane binding regulate c-Src stability and kinase activity. *Mol Cell Biol* **30**, 4094–4107.
[34] Kim S, Alsaidan OA, Goodwin O, Li Q, Sulejmani E, Han Z, Bai A, Albers T, Beharry Z, and Zheng YG, et al (2017). Blocking myristoylation of Src inhibits its kinase activity and suppresses prostate cancer progression. *Cancer Res* **77**, 6950–6962.
[35] Bluemn EG, Coleman IM, Lucas JM, Coleman RT, Hernandez-Lopez S, Tharakan R, Bianchi-Frias D, Dumpit RF, Kaipainen A, and Corella AN, et al (2017). Androgen receptor pathway-independent prostate cancer is sustained through FGF signaling. *Cancer Cell* **32**, 474–489 [e476].
[36] Katoh Y and Katoh M (2009). FGFR2-related pathogenesis and FGFR2-targeted therapeutics (Review). *Int J Mol Med* **23**, 307–311.
[37] Ranieri D, Rosato B, Nanni M, Magenta A, Belleudi F, and Torrisi MR (2016). Expression of the FGFR2 mesenchymal splicing variant in epithelial cells drives epithelial-mesenchymal transition. *Oncotarget* **7**, 5440–5460.
[38] Savagner P, Valles AM, Jouanneau J, Yamada KM, and Thiery JP (1994). Alternative splicing in fibroblast growth factor receptor 2 is associated with induced epithelial-mesenchymal transition in rat bladder carcinoma cells. *Mol Biol Cell* **5**, 851–862.
[39] Zhu DY, Guo QS, Li YL, Cui B, Guo J, Liu JX, and Li P (2014). Twist1 correlates with poor differentiation and progression in gastric adenocarcinoma via elevation of FGFR2 expression. *World J Gastroenterol* **20**, 18306–18315.
[40] Qian X, Anzovino A, Kim S, Suyama K, Yao J, Hulit J, Agiostratidou G, Chandiramani N, McDaid HM, and Nagi C, et al (2014). N-cadherin/FGFR promotes metastasis through epithelial-to-mesenchymal transition and stem/-progenitor cell-like properties. *Oncogene* **33**, 3411–3421.
[41] Sandilands E, Akbarzadeh S, Vecchione A, McEwan DG, Frame MC, and Heath JK (2007). Src kinase modulates the activation, transport and signalling dynamics of fibroblast growth factor receptors. *EMBO Rep* **8**, 1162–1169.
[42] Brooks AN, Kilgour E, and Smith PD (2012). Molecular pathways: fibroblast growth factor signaling: a new therapeutic opportunity in cancer. *Clin Cancer Res* **18**, 1855–1862.
[43] Ridyard MS and Robbins SM (2003). Fibroblast growth factor-2-induced signaling through lipid raft-associated fibroblast growth factor receptor substrate 2 (FRS2). *J Biol Chem* **278**, 13803–13809.
[44] Su N, Jin M, and Chen L (2014). Role of FGF/FGFR signaling in skeletal development and homeostasis: learning from mouse models. *Bone Res* **2**, 14003.
[45] Kim S, Yang X, Li Q, Wu M, Costyn L, Beharry Z, Bartlett MG, and Cai H (2017). Myristoylation of Src kinase mediates Src induced and high fat diet accelerated prostate tumor progression in mice. *J Biol Chem* **292**, 18422–18433.
[46] Araujo JC, Trudel GC, Saad F, Armstrong AJ, Yu EY, Bellmunt J, Wilding G, McCaffrey J, Serrano SV, and Matveev VB, et al (2013). Docetaxel and dasatinib or placebo in men with metastatic castration-resistant prostate cancer (READY): a randomised, double-blind phase 3 trial. *Lancet Oncol* **14**, 1307–1316.
[47] Felsted RL, Glover CJ, and Hartman K (1995). Protein N-myristoylation as a chemotherapeutic target for cancer. *J Natl Cancer Inst* **87**, 1571–1573.
[48] Ducker CE, Upson JJ, French KJ, and Smith CD (2005). Two N-myristoyltransferase isozymes play unique roles in protein myristoylation, proliferation, and apoptosis. *Mol Cancer Res* **3**, 463–476.
[49] Thinon E, Serwa RA, Broncel M, Brannigan JA, Brassat U, Wright MH, Heal WP, Wilkinson AJ, Mann DJ, and Tate EW (2014). Global profiling of co- and post-translationally N-myristoylated proteomes in human cells. *Nat Commun* **5**, 4919.
[50] French KJ, Zhuang Y, Schrecengost RS, Copper JE, Xia Z, and Smith CD (2004). Cyclohexyl-octahydro-pyrrolo[1,2-a]pyrazine-based inhibitors of human N-myristoyltransferase-1. *J Pharmacol Exp Ther* **309**, 340–347.